Developmental alignment of feedforward inputs and recurrent network activity drives increased response selectivity and reliability in primary visual cortex following the onset of visual experience.

Augusto A. Lempel and David Fitzpatrick.

Department of Functional Architecture and Development of Cerebral Cortex, Max Planck Florida Institute for Neuroscience, Jupiter, Florida, USA.

Correspondence should be addressed to D.F. (david.fitzpatrick@mpfi.org)

Abstract

Selective and reliable cortical sensory representations depend on synaptic interactions between feedforward inputs, conveying information from lower levels of the sensory pathway, and recurrent networks that reciprocally connect neurons functioning at the same hierarchical level. Here we explore the development of feedforward/recurrent interactions in primary visual cortex of the ferret that is responsible for the representation of orientation, focusing on the feedforward inputs from cortical layer 4 and its relation to the modular recurrent network in layer 2/3 before and after the onset of visual experience. Using simultaneous laminar electrophysiology and calcium imaging we found that in experienced animals, individual layer 4 and layer 2/3 neurons exhibit strongly correlated responses with the modular recurrent network structure in layer 2/3. Prior to experience, layer 2/3 neurons exhibit comparable modular correlation structure, but this correlation structure is missing for individual layer 4 neurons. Further analysis of the receptive field properties of layer 4 neurons in naïve animals revealed that they exhibit very poor orientation tuning compared to layer 2/3 neurons at this age, and this is accompanied by the lack of spatial segregation of ON and OFF subfields, the definitive property of layer 4 simple cells in experienced animals. Analysis of the response dynamics of layer 2/3 neurons with whole-cell patch recordings confirms that individual layer 2/3 neurons in naïve animals receive poorly-selective feedforward input that does not align with the orientation preference of the layer 2/3 responses. Further analysis reveals that the misaligned feedforward input is the underlying cause of reduced selectivity and increased response variability that is evident in the layer 2/3 responses of naïve animals. Altogether, our experiments indicate that the onset of visual experience is accompanied by a critical refinement in the responses of layer 4 neurons and the alignment of feedforward and recurrent networks that increases the selectivity and reliability of the representation of orientation in V1.

Introduction

During the development of sensory cortices, the onset of experience transforms immature cortical networks into mature representations that support reliable discrimination of behaviorally relevant stimuli. The representation of orientation in ferret primary visual cortex (V1) serves as an ideal model system to explore the mechanisms responsible for the development of cortical representations[1]. In ferrets[2], as in most highly visual mammals including primates[3,4], this representation exhibits an orderly spatial topology—a modular clustering of cortical neurons with similar orientation preferences, that is maintained across cortical depth as iso-orientation columns. Such organized representation results from an orderly convergence of ON and OFF inputs from the lateral geniculate nucleus onto individual neurons in cortical layer 4 (L4)[5–8]. L4 neurons then relay this selectivity to recurrently interconnected neurons in layer 2/3 (L2/3) through feedforward connections.

Previous studies have provided evidence that some aspects of this representation are present at the onset of visual experience. When ferrets first open their eyes (visually naïve), responses of neurons in L2/3 to the presentation of oriented gratings show moderate selectivity and form large-scale modular patterns across the neuronal population[2,9–11]. Yet, recent studies have revealed that these modular population responses and the responses of individual neurons, lack the trial-to-trial reliability and degree of selectivity found in the mature cortex[11]. Within a week of visual experience, responses become highly reliable and selective[11], transforming cortical circuits into a mature representation that faithfully encodes stimulus information, which is essential to drive behavior. Despite decades of research on the development of orientation selectivity, we still lack a clear picture of the functional state of feedforward and recurrent connectivity in L2/3 of naïve V1 and the changes these connections undergo after experience to produce a mature representation.

Here, we address this gap in understanding by combining epi-fluorescence calcium imaging and laminar single-unit electrophysiology to resolve the relationship between modular population responses in L2/3 and single-unit responses in L2/3 and L4 before and after visual experience. In experienced animals, single-unit responses in both L2/3 and L4 are highly correlated with modular population responses in L2/3, consistent with both strong co-activity within the L2/3 recurrent network and alignment of the L4 feedforward inputs to L2/3 population responses. In naïve animals, single-unit responses in L2/3 also show strong correlation with population responses in this layer, indicating strong co-activity across the recurrent network. Unexpectedly, at this age, responses of single-units in L4 are not correlated with population responses in L2/3, indicating that feedforward inputs and recurrent connectivity in L2/3 only become aligned after the onset of visual experience. By further exploring the response properties of layer 4 neurons we discovered that orientation selectivity is strikingly weak in L4 of naïve animals, and reverse correlation analysis using m-sequence (white noise) stimuli[12,13] revealed that ON and OFF responses lack the spatial subfield segregation (simple cell structure) that is present following a week of visual experience. By performing in-vivo whole-cell recordings in L2/3 neurons of naïve animals, we confirmed that short-latency feedforward inputs contribute poor orientation selectivity that is misaligned with the cell's overall response. After eye opening, L4 responses develop strong orientation selectivity, due to a developmental spatial segregation of ON and OFF responses. In turn, short-latency feedforward inputs to L2/3 neurons became strongly orientation-selective and aligned with their overall response, resulting in high response reliability.

Altogether, our experiments indicate that the maturation of L4 neuronal responses after the onset of experience results in the alignment of feedforward inputs and population responses in the L2/3 recurrent network increasing the selectivity and reliability of the representation of orientation in L2/3.

Results

In naïve V1, layer 4 responses do not align with modular response patterns in layer 2/3.

To resolve the functional state of feedforward and recurrent connectivity that contributes to modular population responses in L2/3, we began by probing the relationship between these modular responses and single-unit responses in L2/3 and L4 using simultaneous trial-to-trial measurements of both single-unit responses and large-scale activity patterns. To achieve this, we performed epi-scale calcium imaging and laminar electrophysiology simultaneously (Figure 1A). Visually naïve (eyes opened artificially during experiment) and experienced (at least 5 days after eye-opening) ferrets were anesthetized, paralyzed, and presented with oriented, drifting gratings. A non-parametric measure of trial-to-trial correlation (see methods) was then computed between stimulus-evoked calcium responses, indicative of population responses across the L2/3 recurrent network, and single-unit spiking responses in different layers (Figure 1B). Calcium responses were z-scored for each trial to prevent trial-to-trial changes in response amplitude from contributing to the response pattern correlations. Layers were identified using sink-source analysis of local field potentials. The strength and spatial spread of these correlations were quantified as the mean absolute correlation value across imaging pixels and the proportion of pixels with a significant correlation respectively (Figure 1C).

In experienced V1 (Figure 1B-C top rows), single-unit responses in L2/3 showed strong and widespread correlations with calcium responses (Mean correlation strength = 2.4. Mean correlation spread = 0.32), indicating co-activity across the L2/3 recurrent network. Single-unit responses in L4 showed similar correlations to the calcium responses as those in L2/3 (Mean correlation strength = 2. Mean correlation spread = 0.23. Comparison with L2/3; $p = 0.11$ and 0.08 respectively), consistent with functional alignment between feedforward connectivity and population responses across the L2/3 recurrent network.

In naïve animals, L2/3 units showed similar correlation with modular calcium responses as L2/3 units in experienced V1 (Mean correlation strength: 2.35, median spread: 0.32, $p \sim 1$ for both comparisons with experienced L2/3) indicating little impact of early experience on this property of the recurrent network. In contrast, units in L4 showed much weaker correlations (Mean correlation strength: 1.5. Comparison to naïve L2/3: $p < 0.001$. Comparison to experienced L4: $p = 0.05$) that were restricted to a smaller area (Mean correlation spread: 0.11. Comparison to naïve L2/3: $p < 0.001$. Comparison to experienced L4: $p = 0.03$), and did not reflect a large-scale modular pattern (See example in Figure 1B). These data suggest that L4 neurons provide the L2/3 recurrent network with immature feedforward inputs that do not align with its modular population responses at this age.

In naïve V1, layer 4 neurons exhibit weak orientation selectivity and discriminability relative to layer 2/3 neurons.

Given the lack of correlation of L4 neuron responses to the L2/3 recurrent network in naïve animals, this made us question whether L4 neurons were providing L2/3 neurons with tuned feedforward inputs at this age. To test this, we compared orientation selectivity (OS) of single-unit responses across layers. As a reference, we started with experienced animals (Figure 1D-E top rows), where we found similar orientation tuning in L4 and L2/3 (Mean OS; L2/3: 0.57, L4: 0.51. $p = 0.45$), consistent with L2/3 neurons inheriting selectivity from L4 feedforward inputs. In naïve V1 (Figure 1D-E bottom rows), although the selectivity in L2/3 is weaker than that in experienced animals (Mean OS naïve L2/3: 0.37. Comparison to experienced: $p < 0.003$), the selectivity in L4 is significantly less than the L2/3 naïve selectivity (Mean OS naïve L4: 0.17. $p < 0.001$) and strikingly reduced from the values in experienced L4 ($p < 0.001$).

To better appreciate how these differences in selectivity relate to the ability of neurons to discriminate different orientations, we quantified single-unit orientation discriminability as the Cohen's D between single-trial

responses to the preferred and orthogonal orientations (D'. Figure 1E). In experienced animals, discriminability was similar across layers (Mean D'; L2/3: 3.59. L4: 3.5. $p = 0.51$). In contrast, although discriminability of single-unit responses in L2/3 was reduced in the naïve animals (Mean D' in L2/3 of naïve animals: 2.09. Comparison with L2/3 of experienced animals: $p = 0.002$), these neurons were much better at discriminating orthogonal orientations than those in L4 (Mean D' in L4 of naïve animals: 0.88. Comparison with L2/3 of naïve animals: $p < 0.001$). Trial to trial variability is a major factor in discriminability and these results suggest that the lack of correlation of L4 inputs with the recurrent L2/3 network in naïve animals, reflects the unreliable and poorly selective responses of the L4 neurons at this age. It also suggests that the level of selectivity and discriminability that is present in naïve L2/3 neurons depends heavily on recurrent network interactions.

Given the unexpected nature of these laminar differences, we thought it important to rule out other factors that could explain the results. First, we asked if they could be due to differences in stimulus responsiveness across layers. In naïve animals, where strong laminar differences are found, responsiveness to grating stimuli was higher in L4 than L2/3 units (Mean response across stimuli; L2/3: 2.11Hz. L4: 3.74Hz. $p = .02$). Therefore, poor responsiveness of L4 neurons cannot account for their lack of selectivity or correlation with calcium response patterns. Next, we performed additional analysis to test the robustness of our results with respect to the laminar classification of our single-unit data. We analyzed changes in single-unit responses across cortical depth relative to the cortical surface. We found a strong negative correlation between unit's depths and both orientation selectivity and strength of correlation with calcium response patterns for data recorded in naïve but not experienced animals (Figure 2A. $p < 0.001$ for both correlation). When cortical depth was computed relative to the identified L2/3-L4 border, both response properties fell sharply at the laminar border for data in naïve animals but did not vary with cortical depth within the same layer (Figure 2B). This analysis provides confidence in our laminar identification and indicates response properties change with laminar identity and not simply cortical depth.

Overall, our results in experienced animals agree with classic feedforward mechanisms driving orientation selectivity and supporting modular network responses in L2/3. In contrast, data in naïve animals suggest a different state in which a modular recurrent network in L2/3 receives feedforward inputs from L4 that are poorly tuned and do not align with the modular population responses in L2/3. With experience, orientation selectivity emerges in L4, and L4 responses align with L2/3 responses. Our next experiments further characterize the changes in the properties of L4 neurons that enhance their orientation selectivity following visual experience.

<u>Spatial segregation of ON and OFF responses explains increased orientation selectivity in layer 4 neurons after eye opening.</u>

It is well known that the complementary spatial arrangement of ON and OFF lateral geniculate inputs in the simple cell receptive fields of L4 neurons drives orientation selective responses[5–8]. This led us to wonder whether developmental changes in the organization of ON and OFF visual responses of L4 neurons could account for the increased orientation selectivity in this layer after eye opening. For this, we recorded and analyzed responses to randomized m-sequence stimuli[12,13] (Figure 3A).

First, we mapped single-unit linear receptive fields (RF) by computing a latency-corrected spike-triggered stimulus average as in previous studies[12,13] (Figure 3A. See methods for details). This analysis reveals the overall structure of a neuron's RF. Yet, it cannot resolve neuronal responses to increases (ON) and decreases (OFF) of luminance independently. In particular, mapping the RF of a neuron with superimposed ON and OFF responses (an ON-OFF response) results in a single sub-field of whichever polarity elicits the strongest response (see naïve examples in Figure 3B). To get an independent estimate of ON and OFF responses across retinotopic space, we calculated luminance changes between adjacent frames of the m-sequence stimuli and computed a latency-

corrected spike-triggered average for either increases or decreases in local luminance separately (Figure 3A, see methods for details).

At both ages, our analysis yields clear RFs and strong ON and/or OFF responses, indicating L4 activity conveys visual information even before eye opening. Moreover, RFs show similar overall size across ages (Mean size; Naïve: 81deg^2. Experienced: 93deg^2. $p = 0.19$). Yet, striking differences are seen in the relationship between ON and OFF responses and the structure of linear RFs across age groups (Figure 3B).

In experienced animals, ON and OFF responses are spatially segregated consistent with previous studies[5–8]. This segregation results in a Gabor like RF structure optimal for edge detection (see experienced examples in Figures 3A and 3B). In contrast, ON and OFF responses show significant superposition in naïve animals. This superposition results in a RF structure consisting of a single ON or OFF subfield (Figure 3B, naïve examples), ideal for providing local luminance information but suboptimal for edge detection. To quantify this difference in ON-OFF superposition, we computed the correlation between ON and OFF response strength across space (Figure 4A). Correlations are generally negative for data in experienced animals, indicating spatial segregation, and much higher in data from naïve animals, indicating stronger spatial superposition (Mean ON-OFF spatial correlation; Experienced: -0.26. Naïve: 0.07. $p < 0.001$).

In addition to increased spatial superposition in naïve compared to experienced animals, ON and OFF responses are less balanced in their overall strength in the naive, meaning one polarity elicits much stronger responses than the other. We quantified this ON-OFF bias as the difference between the ON and the OFF response strength, averaged across space, divided by the sum (Figure 4B). Data in naïve animals show stronger biases than those in experienced animals (Mean ON-OFF bias; Naïve: 0.62. Experienced: 0.43. $p = 0.004$). In addition, we saw a slight bias for cells to have an OFF preference in naïve but not in experienced animals, though this difference in proportions was not significant (Naïve: 41% ON, 59% OFF. Experienced: 50% ON, 50% OFF. $p = 0.67$).

Overall, our analysis of ON and OFF responses suggest that, after experience, ON-OFF thalamic inputs become more intermixed across cells, decreasing ON-OFF bias. Most importantly, they also become spatially segregated for individual L4 cells after eye opening, resulting in Gabor like receptive fields optimal for edge detection.

In addition to the emergence of complementary ON/OFF spatial organization, we wondered if there were other properties of the receptive field spatial organization that could change with experience and increase selectivity for orientation. Elongation of subfields along the axis of preferred orientation in experienced animals is a factor in enhancing the orientation selectivity[14,15] and so we quantified the circularity of individual ON or OFF sub-fields as the ratio between their minor and major axis (Figure 4C). Note that some cells contributed both an ON and OFF sub-fields, especially in experienced data, and so the n of this analysis is larger than previous ones. Sub-fields display higher circularity in naïve compared to experienced animals (Mean sub-field circularity; Naïve: 0.73. Experienced: 0.59. $p < 0.001$) suggesting they are poorly suited to detect oriented edges.

The presence of segregated and less circular ON and OFF sub-fields in experienced animals should provide L4 neurons with stronger orientation selectivity. To quantify the ability of linear RFs to detect edge orientation, we simulated responses to oriented, drifting gratings, by convolving stimuli with the RF structure and applying a rectifying non-linearity (Figure 4D, see methods for details). We then computed a simulated orientation selectivity for each L4 neuron based on these responses (Figure 4E). Simulated orientation selectivity is much stronger for RF in experienced compare to those in naïve animals (Mean simulated orientation selectivity; Naïve: 0.17. Experienced: 0.3. $p < 0.001$).

Overall, our results indicate that neurons in L4 of naïve V1 provide information on local luminance but not edge orientation signals due to a spatial superposition of ON and OFF responses. Orientation selectivity increases in L4 after experience due to a spatial segregation of such responses.

Feedforward inputs to layer 2/3 neurons become orientation selective and aligned with the layers 2/3 recurrent network after eye opening.

Data thus far illustrate a dramatic increase in the orientation selectivity of single-cell responses in L4 after eye opening, consistent with the enhanced alignment of L4 cell responses with the recurrent modular network patterns in L2/3. But to better understand the relation between the changing properties of L4 neurons and the activity patterns in L2/3, we turned to an analysis of the dynamic properties of the integrated synaptic inputs received by individual L2/3 cells and how these change with experience. We achieved this by performing *in-vivo* whole cell recordings in L2/3 (Figure 5A) of naïve and experienced animals and measuring sub-threshold responses to drifting grating stimuli as described for data in Figure 1.

Shortly after stimulus onset, L2/3 neurons receive stimulus-evoked feedforward inputs. As time progresses, recurrent connections between L2/3 neurons shape responses across the network to produce modular activity (see Figure 1). Thus, the functional relationship between feedforward inputs and modular activity in the L2/3 recurrent network can be assessed by comparing functional properties of the input received by L2/3 cells at different latencies. For each cell, we first corrected responses by their onset latency to prevent differences across neurons in response onset latency from impacting our analysis of response dynamics (Figure 5B. see methods for details). We then computed a "full response" as the temporal averaged response across 1 sec following response onset. Only cells that displayed robust orientation discriminability ($D' \geq 1$) in their full response were considered for further analysis. Next, we computed 100msec long responses at 10 different latencies, relative to response onset, spanning 1 sec. For both the full response and the response at each latency, we computed multiple functional properties that we discuss in the following paragraphs. To test for changes in response properties across latencies as well as differences in the dynamics of these properties across age groups we used repeated measures analysis of variance.

First, we asked if the onset latency and overall strength of sub-threshold responses is different across development. Sub-threshold responses show similar overall strength (Mean response; Naïve: 5.29mV. Experienced: 5.33mV. $p = 0.79$) and onset latency (Mean latency; Naïve: 51msec. Experienced: 43msec. $p = 0.25$) across age groups. Next, we tested for differences in response strength at different latencies that may confound our analysis of response properties dynamics. While response strength increased with latency at both ages (naïve p: 0.05, experienced $p < 0.001$), this modulation was moderate and response strength did not fall below 80% of that for the full response at any latency in either age group (Figure 5C). Thus, any differences in response properties between latencies and age groups are unlikely to be caused by differences in overall response strength.

Next, we asked if the contribution of feedforward inputs to the orientation selectivity of individual L2/3 cells changes across development. To resolve this, we analyzed temporal changes in orientation selectivity of sub-threshold responses (Figure 5D). In experienced animals, orientation selectivity did not change with latency (p: 0.32), indicating full support of feedforward inputs to the cell's response selectivity at this age. Notably, data from naïve animals showed weak orientation selectivity in the earliest response, providing further evidence that feedforward inputs are poorly tuned and cannot explain response selectivity in L2/3 cells at this age. Orientation selectivity of the sub-threshold responses in naïve animals improved with increasing latency ($p < 0.001$. Difference in dynamics with experienced, $p < 0.001$), plateauing around 500msec, consistent with orientation selectivity in naïve animals emerging from recurrent network dynamics in L2/3.

To test whether feedforward inputs become functionally aligned with L2/3 recurrent network responses after eye opening, we calculated the difference in orientation preference between sub-threshold responses at different latencies and the full response of the cells (Figure 2E). In experienced animals, response at the earliest latency already shows good preference matching with the full response. This matching improves only marginally, though significantly ($p = 0.005$), with increased latency, plateauing at 200msec. These data suggest good, though not perfect, alignment between stimulus preference of feedforward inputs and the L2/3 recurrent network at this age. In naïve animals, response at the earliest latency shows a much larger orientation preference mismatch to that of the full response when compared to the same latency in experienced animals (Mean mismatch at 0msec latency; Experienced: 13deg. Naïve: 35deg. $p < 0.001$.). This mismatch was then reduced with increased latency ($p < 0.001$) plateauing at 500msec. Overall, these results indicate that feedforward inputs become aligned with orientation-selective responses in the L2/3 recurrent network after eye opening.

In computational neural networks, increased alignment of feedforward inputs to recurrent connectivity results in increased reliability of the network's responses[11], a phenomena related to recurrent amplification[16–20]. If this is true for the biological recurrent network in L2/3 of V1, we should observe a decrease in variability with increased latency for experienced animals, as recurrent interactions will stabilize the initial responses elicited by feedforward inputs. In contrast, this decrease in variance should not manifest in L2/3 cell of naïve animals for which feedforward inputs and recurrent connectivity show strong misalignment. To test this, we calculated response Fano factor, as the trial-to-trial response variance divided by the trial-averaged response amplitude, for the preferred stimulus at different latencies in experienced and naïve animals (Figure 2F). Indeed, we find that Fano factor decreases with latency in experienced ($p < 0.001$) but not naïve animals ($p = 0.66$. Difference in dynamics with experienced, $p = 0.003$), consistent with functional alignment of feedforward inputs and recurrent connections impacting the ability of the L2/3 recurrent network to produce reliable responses.

The ability of the cortical network to provide useful information to drive behavior ultimately depends on the power of neuronal activity to discriminate different stimuli. This can be quantified by the Cohens D' between responses to preferred and non-preferred stimuli (D'. Figure 5G). D' depends on both the difference in mean responses across stimuli as well as their trial-to-trial variance and is therefore affected by both response selectivity and variability. We then asked how changes in both response selectivity and variability contributed to D' at different latencies and across age groups.

For the earliest latency, D' was already much larger in experienced than naïve animals (Mean D' at 0msec; Experienced: 2.08. Naïve: 1.19. $p = 0.009$). Yet, Fano factor was comparable across age groups at this latency (Mean Fano factor at 0msec; Experienced: 0.53. Naïve: 0.43. $p = 0.5$). Therefore, the initial difference in D' between age groups is due to more selective yet similarly variable feedforward inputs after eye opening. For longer latencies, D' increased in both naïve ($p = 0.005$) and experienced animals ($p < 0.001$), though for different underlying reasons. While in naïve animals this is driven by an increase in response selectivity (Figure 5D), it was driven by decreased variability in the experienced animals (Figure 5F).

In sum, stimulus discriminability increases with experience due to both an increase in feedforward selectivity and increased feedforward-recurrent alignment, which reduces response variability. Both of these changes likely result from the maturation of L4 responses seen in our previous experiments, which would then be the underlying cause of increased selectivity and reliability of the representation of orientation in V1 that emerges after the onset of experience.

Discussion

Here, we present data from a variety of techniques including: simultaneous laminar electrophysiology and calcium imaging; receptive field mapping analysis; and in-vivo whole cell recordings, to resolve the properties of neuronal responses in recurrently connected L2/3 and its relationship to feedforward inputs provided by neurons in L4 before and after the onset of visual experience. The most striking conclusion from our experiments is that before experience, poorly orientation-selective L4 neurons provide misaligned feedforward inputs to a mature, modular recurrent network in L2/3. The emergence of strong orientation selectivity in L4 neurons after eye opening produces a maturation of feedforward inputs to L2/3 which become aligned to the recurrent network resulting in a highly reliable representation of edge orientation in V1.

<u>Layers 2/3 orientation selectivity becomes supported by feedforward inputs after eye opening:</u>
Our data in experienced animals agrees with classic feedforward mechanisms of orientation selectivity[5–8]. L4 receptive fields display a Gabor-like structure that produces strong selectivity in this layer which is then inherited by L2/3 through strongly selective feedforward inputs. In contrast, in naïve V1, L4 receptive fields show superimposed ON and OFF responses, L4 responses show much weaker orientation selectivity compared to those in L2/3 at this age, and short-latency feedforward inputs to L2/3 cells do not match the neurons orientation preference nor their degree of selectivity. These results reject the established view that the representation of orientation in V1 originates from endogenously generated biases in feedforward connectivity, and in particular thalamic inputs to L4 neurons, before visual experience[21–27]. In fact, our L4 receptive field data strongly suggests a profound re-wiring of thalamic input after eye opening. It's important to recognize that L4 neurons receive intra-cortical inputs as well as thalamic inputs[28,29] and thus changes in RF structure likely reflect changes in both connections. Still, previous studies show that the orientation selectivity and overall RF structure of L4 neurons derives from thalamic inputs[5–8], while intra-cortical connections provide further sharpening of tuning and extra-classical RF properties[30,31].

In light of the inconsistency of our findings with classic feedforward mechanisms driving orientation selectivity in L2/3 of naïve V1, we explored alternative sources for this selective signal. We first considered a direct feedforward input to L2/3 from high-latency, orientation selective neurons in the lateral geniculate nucleus (LGN), akin to those in the koniocellular layers of cat[32] and primate thalamus[33–35]. Previous studies indicate a response latency of orientation selective cells in ferret LGN of about 20-40msec[36], which is not long enough to explain a 500msec-long emergence of selectivity in L2/3 sub-threshold responses. Another hypothesis that could explain the long latency onset of selectivity in L2/3 is a dynamic feedforward-feedback loop interaction with higher-order areas. While we cannot definitively disprove this hypothesis, as it would require a global inactivation of all possible sources of feedback, top-down mechanisms are unlikely under the anesthesia conditions in our experiments, which have been shown to have deleterious effects on higher-order processing in general and top-down interactions in particular[37,38]. Instead, the mechanism that best explains our data is that the recurrent network in L2/3 generates strong orientation selective signals by amplifying specific patterns of weakly selective feedforward input provided by L4 neurons[11,17–20].

<u>Feedforward inputs from layer 4 to layers 2/3 become aligned with the layer 2/3 recurrent network after eye opening:</u>
The prevailing view of cortical development is that endogenous mechanisms set up an initial organization of feedforward connectivity that matures with visual experience[21–27]. Recurrent connections, which undergo extensive refinement after the onset of experience[39], are thought to mature only after feedforward connections are established. Our observations challenges this view by demonstrating substantial functional organization in the recurrent, modular network in L2/3 of V1 in naïve animals. Evidence of this is a modest degree of orientation

selectivity and strong correlations between single-unit activity and large-scale, modular population responses in L2/3. This occurs in spite of the fact that L4 neurons have little orientation selectivity and do not supply feedforward inputs that align with the recurrent network. This suggests a different developmental sequence for the emergence of robust cortical representations. First, recurrent networks establish an initial modular network structure prior to the onset of experience. Later, experience produces strong orientation tuning in L4 neurons and aligns the feedforward inputs they project to L2/3 with recurrent connectivity, transforming the initial modular structure into a mature representation of orientation.

Enhanced reliability of responses in layer 2/3 emerges from alignment of feedforward and recurrent circuits:
A recent study proposes that the lack of reliability in V1 modular responses seen before eye opening is explained by the misalignment between feedforward inputs and recurrent connections at this age[11]. In this conception, variability emerges from a stochastic component of recurrent amplification mechanisms[17–20], which have been shown to operate in L2/3[16]. As initial experimental evidence for this hypothesis, the authors show that responses to visual stimuli that closely resemble spontaneous activity, which suggest strong feedforward-recurrent alignment, display higher reliability[11]. Our in-vivo whole-cell data shows that, in experienced animals, aligned feedforward-recurrent connections increase the reliability of long-latency responses. In contrast, response variance in L2/3 cells of naïve animals, where feedforward inputs are misaligned with recurrent connectivity, was not reduced at longer latencies. These results provide stronger and more direct evidence that increased alignment between feedforward inputs and recurrent connections underlies increased reliability of responses to oriented edges in V1 after eye opening.

Developmental changes in feedforward connectivity recapitulate changes in vision:
Eye opening is a pivotal event in vision development due to the changes it generates on the visual input received by the retina. Under closed eye-lids, the retina is exposed to diffuse light preventing the visualization of edges but permitting that of regional luminance changes. After eye opening, the animal is suddenly exposed to images composed of sharp edges at different orientations. Our data reveals a transformation of L4 receptive fields following eye opening that mirrors such changes in vision. In naïve V1, L4 receptive fields are optimized to detect local luminance while in experienced animals their structure is optimal for detecting oriented edges. Similarly, feedforward inputs to L2/3 become aligned with modular population responses to oriented gratings (i.e. edges) after eye opening. The transformations described here for responses to oriented gratings likely represent a specific instance of a more general developmental mechanism. As the cortex matures, feedforward connections are re-wired to align the input structure elicited by early sensory experience (nurture) with an endogenously generated structure of recurrent connectivity (nature).

Conclusions
Our experiments call for a major revision in established, purely feedforward models for the development of orientation maps in V1. We propose a new paradigm where, at eye opening, first exposure to oriented edges elicit poorly selective responses in L4 due to an immature arrangement of thalamic inputs. L4 then provides poorly selective feedforward inputs to a mature L2/3 recurrent network that produces modular population responses and amplifies orientation selectivity. Yet, a misalignment between feedforward inputs and recurrent connectivity produces highly variability in L2/3 responses. With experience, the maturation of orientation selectivity in L4 produces selective feedforward inputs that align with recurrent connectivity in L2/3 resulting in a highly selective and reliable representation of edge orientation in V1.

Methods

Experimental Model and Subject Details: All experimental procedures were approved by the Max Planck Florida Institute for Neuroscience Institutional Animal Care and Use committee and were performed in accordance with guidelines from the U.S. National Institute of Health. Juvenile female ferrets from Marshal Farms were co-housed with jills on a 16-h light/8-h dark cycle.

Intra-cranial virus injections: For experiments involving calcium imaging, viral injections were performed as previously described[10,40]. Briefly we expressed GCaMP6s[41] or JrGeco1a[42] by microinjection of AAV2/1-hSyn-GCaMP6s/JrGeco1a-WPRE-SV40 (University of Pennsylvania Vector Core or Addgene®) into the visual cortex 1-4 weeks before imaging experiments. In developing ferrets, viral expression using the Synapsin promoter has previously been demonstrated to primarily label excitatory neurons[43] and yield multiple millimeters of roughly uniform labeling[9]. Anesthesia induction was performed using either ketamine (50mg/kg, IM) and/or isoflurane (1%–3%) delivered in O2 and then maintained with isofluorane (1%–2%). Atropine (0.2mg/kg, IM) was administered to reduce secretions, while Buprenorphine (0.01mg/kg, IM) and a 1:1 mixture of lidocaine and bupivacaine (injected directly into the scalp) were administered as analgesics. Animal temperatures were maintained at 37ºC using a homeothermic heating blanket. Animals were also mechanically ventilated and both heartrate and end-tidal CO2 were monitored throughout the surgery. Under aseptic surgical technique, a small craniotomy was made over visual cortex 4-7 mm lateral and 1-3mm anterior to lambda. 1ul of virus was pressure infused into the cortex through a pulled glass pipette at a single depth of 200-500um in up to 3 locations. This procedure reliably produced robust and widespread expression in excitatory neurons over an area that was always larger than 2mm in diameter.

Surgical preparation: All animals were anesthetized and prepared for surgery as described above. Skin and muscle overlying visual cortex were reflected and a custom-designed metal headplate (8mm DIA) was implanted over the injected region with MetaBond (Parkell Inc.). Then a craniotomy and a subsequent durotomy were performed, and the underlying brain stabilized with agarose (2-3%). The headplate was covered with a thin 8mm coverglass (Warner Instruments) with a drilled hole for access with electrophysiology prove or whole-cell pipette. Coverslip was fixed in place using a stainless-steel retaining ring (5/16'' internal retaining ring, McMaster-Carr). Eye-lids were retracted to open the eyes and Phenylephrine (1.25%–5%) and tropicamide (0.5%) were applied to retract the nictitating membrane and dilate the pupil. Small amount of silicon oil was applied to the eyes to prevent eye drying and irritation. Prior to data collection, isoflurane levels were reduced from a surgical plane to .5-1.2%. After reaching a stable, anesthetic baseline (heart rate of 260-300bpm), animals were paralyzed with pancuronium bromide (0.1-0.4 mg/kg/hr in lactated Ringer's with 5% dextrose, delivered IV). After data acquisition was completed, isoflurane was raised to 5% and animal was given Euthasol (0.5ml, IV or IP) for euthanasia.

Calcium imaging data acquisition: Animal was placed under epi-fluorescent microscope featuring Long-distance 4X Achrovid™ objective, Andor® Zyla 5.5 sCMOS camera, Thorlabs® LEDs and EPI optical path setups. Images were acquired at 10-30Hz depending on the calcium indicatory and expression levels but analyzed as 1 second temporal averages in all cases. Images covered an area approximately 6x6mm square and, after spatial down-sampling, yielded 515x512 pixels. Imaging data was analyzed only for pixels within the area of cortex that displayed strong expression of calcium indicator.

Extracellular electrophysiology data acquisition: For extracellular electrophysiology, silicon probes were provided by Dr. Masmanidis at UCLA[44]. For simultaneous epi-fluorescence imaging and electrophysiology, linear probes with 32 channel spanning 920um depth were used. Layer 4 receptive field data also includes recordings with 64 channel proves spanning 1575um depth. For simultaneous epi-fluorescence imaging and electrophysiology, probe was placed on V1 within the area of highest expression of calcium indicator using a

micro-manipulator. For all experiments, probe was drove down into the cortex until only the most superficial channels, or no channels, were out of the brain. Electrophysiology data was acquired using a Neuralynx® Digital Lynx 4SX system. For temporal alignment of electrophysiology data, imaging data, and stimulus, frame TTL triggers from the sCMOS camera and stimulus TTL triggers from the visual stimulation computer were recorded through the electrophysiology hardware.

Sink-source-analysis of local-field potentials for laminar identification: To identify laminar borders in our multi-channel electrophysiology data we first computed local-field-potentials (LFP) in response to either full-screen changes in luminance or m-sequence stimuli. LFP responses were then band-pass filtered between 5-50Hz, which reliably yielded clean signals in our recordings. We then run a sink-source-density analysis on these responses as described in previous studies[38,45]. We identified the border between layers 2/3 and layer 4 as the most superficial sink-source dipole. The deeper end of layer 4 was estimated as the point of reversal for such dipole. Experiments where this analysis did not yield a clear estimate of laminar borders were discarded.

In-vivo whole cell data acquisition: We followed similar methods for in-vivo whole-cell recordings as described in previous studies by our lab[40,46]. Briefly, recordings were performed by inserting a pipette through the hole of the coverglass into the agarose-filled craniotomy. A silver chloride reference electrode was inserted into the muscle. Recordings were made in current clamp mode. Pipette resistance was 5-8 MΩ. Internal solution contained (in mM) 110 K gluconate, 20 Na-Gluconate, 4 KCl, 10 HEPES, 10 K2-Phosphocreating, 4 Mg-ATP, 0.3 Na3GTP. pH was set to 7.2 and osmolality to ~295 mOsm. Neurons were recorded from layers 2/3 (100 to 400 µm below the pia) using a Multiclamp 700B (Molecular Devices). Series resistance for recordings typically ranged from 20 to 80 MΩ. Analog signals were digitized using Spike2 (CED) and analyzed using custom made MATLAB® based software. Our experiments involved passive measurements of voltage changes with no injection of current and thus online resistance compensation was not required. Online compensation of pipette capacitance often lead to oscillatory current injections and cell damage under our experimental conditions. Considering that our analysis of sub-threshold response dynamics was restricted to 100msec temporal averages, we did not deem such compensation necessary as it only affects dynamics on a timescale shorter than 10msec[47]. Still, the lack of pipette capacitance compensation may have caused a slight over-estimation of the onset latency for sub-threshold responses.

Visual stimulation: Visual stimuli were delivered on a LCD screen placed approximately 20–25cm in front of the eyes using PsychoPy[48]. To evoke orientation responses, full-field square gratings at 100% contrast, 0.06 cycles per degree spatial frequency, and drifting at 3Hz temporal frequency were presented. 8 stimulus orientation and 16 corresponding drifting directions were sampled. In addition, 'blank' stimuli of 0% contrast were presented but not included in any analysis. Stimuli were randomly interleaved and presented for 1s followed by 3-5s of gray screen. 5-10 trials of each stimulus, including blank, was shown.
For receptive field analysis, m-sequence stimuli consisted of 1-minute-long sequences of frames displayed at 2-3Hz temporal frequency. Each frame contained either 50x50 or 100x100 pixels covering 100x100 degrees of visual space. Pixel size was thus 1-4 deg^2. For each frame, pixels were randomly assigned a luminance value of -1 (black) or 1 (white) keeping the number of pixels equal across luminance values. For each experiment, 20-30 such sequences were shown, with a 5 seconds gray screen period between sequences.

Calcium imaging data analysis: Epi-scale calcium responses were computed for each stimulation trial as:

$$\text{Response} = \frac{\mathrm{F_{stim}} - \mathrm{F_{pre}}}{\mathrm{F_{pre}}}$$

Where $\mathrm{F_{stim}}$ is the temporally averaged fluorescence during visual stimuli (1 second long) and $\mathrm{F_{pre}}$ is the temporally averaged fluorescence during the previous second.

Extracellular electrophysiology data analysis: Spike-detection, single-unit isolation, and response analysis was all done with custom MATLAB® based software used in previous studies[49,50]. Spiking responses were computed for each stimulation trial as the difference in firing rate during stimulation (1 second) and that during the previous second.

Analysis of calcium-spikes response correlation: Only imaging pixels corresponding to an area within a 1mm distance from the electrode insertion site were considered for this analysis. This allowed us to assess correlations between single-unit spiking and calcium responses across a similar distance for different experiments where the spread of calcium indicator expression vary. Experiments where the spread of expression was not enough to cover an area of at least 1mm radius were discarded.

Due to both imaging and spiking data not displaying normal distributions, we decided to compute a non-parametric estimator of correlation. First, we z-scored calcium responses across pixels for each trial. This step allowed us to remove any correlations due to overall responsiveness of the cortex and instead isolate correlations based on the modular pattern of calcium activity. Then, for each single-unit recorded during an experiment, we computed a trial-to-trial spike-weighted average of the calcium response acquired at the same experiment. Next, we computed a shuffle distribution of this spike-weighted average by randomly re-assigning spiking responses across trials. 1000 iterations of this randomization were made to compute the distribution. Finally, the non-shuffled spike-weighted averaged was z-scored by the shuffle distribution. Thus, the sign of this quantification represents the sign of the correlation while the absolute amplitude represents the deviation from a randomized expectation based on the data for each experiment and single-unit. Correlations with absolute values above 3 (i.e., more than 3 standard deviations away from the mean of the random distribution) were considered significant. The strength and spatial spread of these correlations was then computed as the mean absolute value of the non-parametric correlations and the proportion of pixels with significant correlations respectively.

Analysis of spiking response orientation selectivity and discriminability: Orientation selectivity was computed based on stimulus responses averaged across trials using a circular variance based metric[51]. To prevent differences in direction selectivity across single-units to affect our quantification of orientation selectivity, responses to gratings drifting on directions opposite to, i.e., more than 90deg away from, that of the preferred stimulus (eliciting the largest response) were not included in the analysis. The equation for the metric was:

$$\mathrm{OS} = \frac{\sqrt{(\sum_{\mathrm{stim}} \sin(\mathrm{Ori}_{\mathrm{stim}} * 2) * \mathrm{Response}_{\mathrm{stim}})^2 + (\sum_{\mathrm{stim}} \cos(\mathrm{Ori}_{\mathrm{stim}} * 2) * \mathrm{Response}_{\mathrm{stim}})^2}}{\sum_{\mathrm{stim}} \mathrm{Response}_{\mathrm{stim}}}$$

Were Ori is the orientation of the stimulus.

Orientation discriminability was computed as the Cohen's D between responses to the preferred grating stimulus (considering both grating orientation and direction) and the two orthogonal gratings (moving in opposite directions). The equation was:

$$\mathrm{D}' = \frac{\mathrm{meanR}_{\mathrm{Pref}} - \frac{\mathrm{meanR}_{\mathrm{Pref+90}} + \mathrm{meanR}_{\mathrm{Pref-90}}}{2}}{\mathrm{stdR}_{\mathrm{Pref}} + \frac{\mathrm{stdR}_{\mathrm{Pref+90}} + \mathrm{stdR}_{\mathrm{Pref-90}}}{2}}$$

Were meanR is the mean response across trials, stdR the standard deviation of trial-to-trial responses, Pref represents the preferred stimulus and $\mathrm{Pref} + 90$ and $\mathrm{Pref} - 90$ represent the two orthogonal gratings moving in opposite directions.

Analysis of layer 4 receptive fields: First, we computed the response latency of each neuron by calculation its spiking response in 33msec temporal windows at different latencies following the onset of each frame in the m-

sequence stimulus. The earliest time bin to show a significant increase in spiking relative to a 33msec temporal window right before frame onset was set to be the neurons latency. Significance was defined as $p < 0.001$ using Wilcoxon Rank Sum test for responses across all frames shown during the experiment at the different temporal bins. For the following analysis, we corrected spikes timing by the response latency.

After latency correction, we computed the spike-triggered average of the m-sequence stimuli (smoothed by a 2-dimensional Gaussian filter of $\sigma = 2$deg). This yielded a 100x100deg stimulus average. We then looked for the 25deg dimeter circular area within this stimulus average that displayed strongest absolute luminance value (strongest ON-OFF signal). Pixels within this circular area were considered inside of the local receptive field of the neuron and all other pixels were considered outside. To quantify the strength of the ON-OFF receptive field, we z-scored the spike-triggered-average luminance values of pixels inside the deceptive field by the distribution of such values in pixels outside the receptive field. Neurons for which the absolute z-scored luminance averaged across all pixels within the receptive field was lower than 1.5 were discarded from analysis.

Analysis of layer 4 ON-OFF responses: For cells that passed our criterion for receptive field strength, we then computed independent ON and OFF responses. First, the difference in luminance across adjacent frames of the m-sequence stimuli (after smoothing) was computed. To compute the ON response, for each pixel in the m-sequence stimuli we identified the frames for which its luminance increased. We then computed a spike-triggered average of these values. As a result, the spike-triggered value for each pixel was higher when the neuron increased it's spiking for larger positive changes in luminance and lower in the opposite case. To compute the OFF response, we followed the same procedure but considering only decreases in luminance. As for receptive field analysis, we then z-scored the spike-triggered-average ON or OFF response of pixels inside the receptive field by the distribution of such values in pixels outside the receptive field. Two neurons recorded in experienced animals that passed our criterion for strong receptive fields did not show strong ON/OFF responses at the same location for this analysis and were discarded.

Analysis of layer 4 ON-OFF response properties: All properties of ON-OFF responses and linear receptive fields were computed based only on the pixels within the receptive field, which formed a 25degree diameter circular area. Thus, our results reflect only the structure of local/classic receptive field structure.

For ON-OFF correlation we computed the Pearson correlation between the ON and the OFF response (reversing the sign of the OFF response) across receptive field pixels.

For ON-OFF bias we computed the averaged ON and OFF response across receptive field pixels (reversing the sign of the OFF response) and computed their difference over their sum. A bias of 1 represents complete dominance of one luminance change polarity while a bias of 0 represents equal strength of the ON and OFF responses.

Analysis of layer 4 ON-OFF subfield circularity: To compute sub-field circularity, we first identified the pixels belonging to either the ON or the OFF sub-field of each receptive field. For this, we draw a polygon around the largest group of neighboring pixels with a z-scored luminance value above 2.5 (for ON sub-field) or below -2.5 (for OFF sub-field). If the resulting polygon for either polarity had an area smaller than 15deg^2, the sub-field was discarded and the receptive field was considered to not have a significant sub-field of that polarity. We then computed the major and minx axis length of the polygons using the MATLAB® function 'regionprops'. Finally, we calculated sub-field circularity as the ration between the minor and major axis lengths.

Simulation of layer 4 receptive field orientation selectivity: To estimate the ability of layer 4 receptive fields to detect edge orientation, we simulated responses to square wave gratings by convolving such stimuli with the luminance values of the pixels in the receptive field. Gratings luminance value range from -1 to 1 and their spatial frequency matched that used in our other experiment (0.06 cycles/degree). To provide good stimulus resolution, pixel size was set to .5x.5 degrees. The resolution or receptive fields was increased through linear extrapolation

to match the stimulus resolution. The same 8 orientations were probed as those used in other experiments. To simulate the temporally averaged response to drifting gratings, we simulated static responses for gratings at 16 different phases (in 22.5deg steps) for each orientation. Responses were then rectified and averaged across phases, yielding a single response for each orientation. Using these simulated responses, we then compute orientation selectivity using circular variance metrics as described previously for spiking responses.

Analysis of whole-cell sub-threshold responses: First, we computed the response latency of each neuron as the time when its membrane potential increased significantly form that during the 10msec prior to stimulus onset considering data across all trials. Statistical significance was defined as $p < 0.001$ using paired t-tests. After correcting sub-threshold responses by this latency, we computed a full response for each trial as the difference in membrane potential between a one second period right after response onset and a one second period preceding response onset. Next, we computed responses for 10 different latencies (0 to 900msec in steps of 100msec) as the difference in membrane potential between a 100msec second period at different delays (according to latency) from response onset and a one second period preceding response onset.

Analysis of whole-cell sub-threshold response properties: For responses at all latencies as well as the full response, orientation selectivity and discriminability were computed using the same formulas as described previously for spiking responses. Fano factor was computed as the standard deviation of trial-to-trial responses to the preferred grating stimulus (considering both orientation and direction) divided by the mean response across trials. To calculate the orientation preference of these responses (Figure 5E) we computed their circular mean as:

$$Preferred\ orientation = tan^{-1}\left(\frac{(\sum_{\text{stim}} \cos(\text{Ori}_{\text{stim}} * 2) * \text{Response}_{\text{stim}})^2}{(\sum_{\text{stim}} \sin(\text{Ori}_{\text{stim}} * 2) * \text{Response}_{\text{stim}})^2}\right)$$

Were Ori is the orientation of the stimulus.

Statistics: For all comparisons in response properties across layers and age groups (all comparison in figures 1 and 4) we used Wilcoxon Rank Sum tests. For changes in response properties across both latency and age groups (Figure 5) we used repeated measures analysis of variance (ANOVA).

References

1. Sharma, J. & Sur, M. The Ferret as a Model for Visual System Development and Plasticity. in *Biology and Diseases of the Ferret* 711–734 (Editors JG Fox and RP Marini, John Wiley and Sons, 2014). doi:10.1002/9781118782699.ch30.

2. Chapman, B., Stryker, M. P. & Bonhoeffer, T. Development of Orientation Preference Maps in Ferret Primary Visual Cortex. *J. Neurosci.* 16, 6443–6453 (1996).

3. Hubel, D. H. & Wiesel, T. N. Sequence regularity and geometry of orientation columns in the monkey striate cortex. *J. Comp. Neurol.* 158, 267–293 (1974).

4. McLoughlin, N. & Schiessl, I. Orientation selectivity in the common marmoset (Callithrix jacchus): The periodicity of orientation columns in V1 and V2. *NeuroImage* 31, 76–85 (2006).

5. Jin, J., Wang, Y., Swadlow, H. A. & Alonso, J. M. Population receptive fields of ON and OFF thalamic inputs to an orientation column in visual cortex. *Nat. Neurosci.* 14, 232–238 (2011).

6. Hubel, D. H. & Wiesel, T. N. Receptive fields, binocular interaction and functional architecture in the cat's visual cortex. *J. Physiol.* 160, 106-154.2 (1962).

7. Chapman, B., Zahs, K. R. & Stryker, M. P. Relation of cortical cell orientation selectivity to alignment of receptive fields of the geniculocortical afferents that arborize within a single orientation column in ferret visual cortex. *J. Neurosci. Off. J. Soc. Neurosci.* 11, 1347–1358 (1991).

8. Mooser, F., Bosking, W. H. & Fitzpatrick, D. A morphological basis for orientation tuning in primary visual cortex. *Nat. Neurosci.* 7, 872–879 (2004).

9. Smith, G. B., Hein, B., Whitney, D. E., Fitzpatrick, D. & Kaschube, M. Distributed network interactions and their emergence in developing neocortex. *Nat. Neurosci.* 21, 1600–1608 (2018).

10. Chang, J. T., Whitney, D. & Fitzpatrick, D. Experience-Dependent Reorganization Drives Development of a Binocularly Unified Cortical Representation of Orientation. *Neuron* 107, 338-350.e5 (2020).

11. Trägenap, S., Whitney, D. E., Fitzpatrick, D. & Kaschube, M. The nature-nurture transform underlying the emergence of reliable cortical representations. 2022.11.14.516507 Preprint at https://doi.org/10.1101/2022.11.14.516507 (2023).

12. Usrey, W. M., Sceniak, M. P. & Chapman, B. Receptive Fields and Response Properties of Neurons in Layer 4 of Ferret Visual Cortex. *J. Neurophysiol.* 89, 1003–1015 (2003).

13. Reid, R. C., Victor, J. D. & Shapley, R. M. The use of m-sequences in the analysis of visual neurons: linear receptive field properties. *Vis. Neurosci.* 14, 1015–1027 (1997).

14. Gardner, J. L., Anzai, A., Ohzawa, I. & Freeman, R. D. Linear and nonlinear contributions to orientation tuning of simple cells in the cat's striate cortex. *Vis. Neurosci.* 16, 1115–1121 (1999).

15. Sasaki, K. *et al.* Supranormal orientation selectivity of visual neurons in orientation-restricted animals. *Sci. Rep.* 5, 16712 (2015).

16. Peron, S. *et al.* Recurrent interactions in local cortical circuits. *Nature* 579, 256–259 (2020).

17. Christie, I. K., Miller, P. & Van Hooser, S. D. Cortical amplification models of experience-dependent development of selective columns and response sparsification. *J. Neurophysiol.* 118, 874–893 (2017).

18. Douglas, R. J., Koch, C., Mahowald, M., Martin, K. A. & Suarez, H. H. Recurrent excitation in neocortical circuits. *Science* 269, 981–985 (1995).

19. Miller, K. D. Canonical computations of cerebral cortex. *Curr. Opin. Neurobiol.* 37, 75–84 (2016).

20. Cossell, L. *et al.* Functional organization of excitatory synaptic strength in primary visual cortex. *Nature* 518, 399–403 (2015).

21. Paik, S.-B. & Ringach, D. L. Retinal origin of orientation maps in visual cortex. *Nat. Neurosci.* 14, 919–925 (2011).

22. Ringach, D. L. Haphazard wiring of simple receptive fields and orientation columns in visual cortex. *J. Neurophysiol.* 92, 468–476 (2004).

23. Schottdorf, M., Keil, W., Coppola, D., White, L. E. & Wolf, F. Random Wiring, Ganglion Cell Mosaics, and the Functional Architecture of the Visual Cortex. *PLOS Comput. Biol.* 11, e1004602 (2015).

24. Schottdorf, M., Eglen, S. J., Wolf, F. & Keil, W. Can Retinal Ganglion Cell Dipoles Seed Iso-Orientation Domains in the Visual Cortex? *PLOS ONE* 9, e86139 (2014).

25. Soodak, R. E. The retinal ganglion cell mosaic defines orientation columns in striate cortex. *Proc. Natl. Acad. Sci.* 84, 3936–3940 (1987).

26. Paik, S.-B. Developmental models of functional maps in cortex. *Biomed. Eng. Lett.* 3, 223–225 (2013).

27. Crair, M. C., Gillespie, D. C. & Stryker, M. P. The role of visual experience in the development of columns in cat visual cortex. *Science* 279, 566–570 (1998).

28. Douglas, R. J. & Martin, K. A. A functional microcircuit for cat visual cortex. *J. Physiol.* 440, 735–769 (1991).

29. Callaway, E. M. Local circuits in primary visual cortex of the macaque monkey. *Annu. Rev. Neurosci.* 21, 47–74 (1998).

30. Li, Y., Ibrahim, L. A., Liu, B., Zhang, L. I. & Tao, H. W. Linear Transformation of Thalamocortical input by Intracortical Excitation. *Nat. Neurosci.* 16, 1324–1330 (2013).

31. Sun, W., Tan, Z., Mensh, B. D. & Ji, N. Thalamus provides layer 4 of primary visual cortex with orientation- and direction-tuned inputs. *Nat. Neurosci.* 19, 308–315 (2016).

32. Shou, T. D. & Leventhal, A. G. Organized arrangement of orientation-sensitive relay cells in the cat's dorsal lateral geniculate nucleus. *J. Neurosci.* 9, 4287–4302 (1989).

33. Eiber, C. D. *et al.* Receptive Field Properties of Koniocellular On/Off Neurons in the Lateral Geniculate Nucleus of Marmoset Monkeys. *J. Neurosci.* 38, 10384–10398 (2018).

34. Cheong, S. K., Tailby, C., Solomon, S. G. & Martin, P. R. Cortical-Like Receptive Fields in the Lateral Geniculate Nucleus of Marmoset Monkeys. *J. Neurosci.* 33, 6864–6876 (2013).

35. Smith, E. L., Chino, Y. M., Ridder, W. H., Kitagawa, K. & Langston, A. Orientation bias of neurons in the lateral geniculate nucleus of macaque monkeys. *Vis. Neurosci.* 5, 525–545 (1990).

36. Murphy, A. J., Hasse, J. M. & Briggs, F. Physiological characterization of a rare subpopulation of doublet-spiking neurons in the ferret lateral geniculate nucleus. *J. Neurophysiol.* 124, 432–442 (2020).

37. Sorrenti, V. *et al.* Understanding the Effects of Anesthesia on Cortical Electrophysiological Recordings: A Scoping Review. *Int. J. Mol. Sci.* 22, 1286 (2021).

38. Sellers, K. K., Bennett, D. V., Hutt, A., Williams, J. H. & Fröhlich, F. Awake vs. anesthetized: layer-specific sensory processing in visual cortex and functional connectivity between cortical areas. *J. Neurophysiol.* 113, 3798–3815 (2015).

39. Durack, J. C. & Katz, L. C. Development of horizontal projections in layer 2/3 of ferret visual cortex. *Cereb. Cortex N. Y. N 1991* 6, 178–183 (1996).

40. Scholl, B., Wilson, D. E., Jaepel, J. & Fitzpatrick, D. Functional Logic of Layer 2/3 Inhibitory Connectivity in the Ferret Visual Cortex. *Neuron* 104, 451-457.e3 (2019).

41. Chen, T.-W. *et al.* Ultra-sensitive fluorescent proteins for imaging neuronal activity. *Nature* 499, 295–300 (2013).

42. Dana, H. *et al.* Sensitive red protein calcium indicators for imaging neural activity. *eLife* 5, (2016).

43. Wilson, D. E. *et al.* GABAergic Neurons in Ferret Visual Cortex Participate in Functionally Specific Networks. *Neuron* 93, 1058-1065.e4 (2017).

44. Yang, L., Lee, K., Villagracia, J. & Masmanidis, S. C. Open source silicon microprobes for high throughput neural recording. *J. Neural Eng.* 17, 016036 (2020).

45. Schaefer, M. K., Hechavarría, J. C. & Kössl, M. Quantification of mid and late evoked sinks in laminar current source density profiles of columns in the primary auditory cortex. *Front. Neural Circuits* 9, 52 (2015).

46. Wilson, D. E., Scholl, B. & Fitzpatrick, D. Differential tuning of excitation and inhibition shapes direction selectivity in ferret visual cortex. *Nature* 560, 97 (2018).

47. Montnach, J. *et al.* Computer modeling of whole-cell voltage-clamp analyses to delineate guidelines for good practice of manual and automated patch-clamp. *Sci. Rep.* 11, 3282 (2021).

48. Brainard, D. H. The Psychophysics Toolbox. *Spat. Vis.* 10, 433–436 (1997).

49. Lempel, A. A. & Nielsen, K. J. Ferrets as a Model for Higher-Level Visual Motion Processing. *Curr. Biol.* 29, 179-191.e5 (2019).

50. Lempel, A. A. & Nielsen, K. J. Development of visual motion integration involves coordination of multiple cortical stages. *eLife* 10, e59798 (2021).

51. Mazurek, M., Kager, M. & Van Hooser, S. D. Robust quantification of orientation selectivity and direction selectivity. *Front. Neural Circuits* 8, (2014).

Figures:

Figure 1

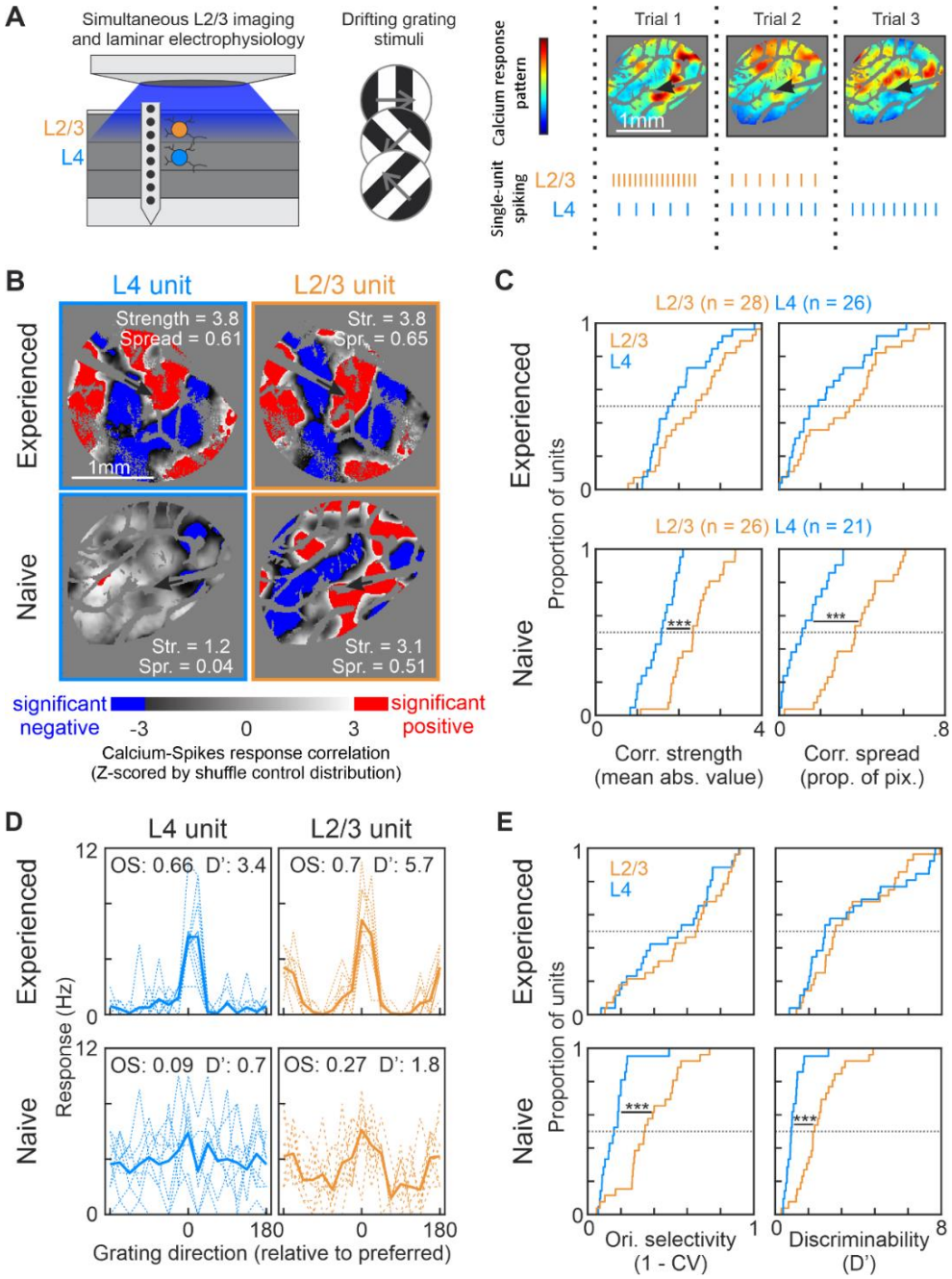

Figure 1: Single-unit responses in layer 4 of naïve V1 do not correlate with population responses in layer 2/3 and display poor orientation selectivity.

(A) Schematic of experimental design, featuring simultaneous epi-scale calcium imaging and laminar, multi-channel, single-unit electrophysiology. Drifting, oriented gratings were presented while measuring single-unit spiking activity in layer 2/3 (L2/3) and layer 4 (L4) and calcium responses across the cortical surface.

(B) Examples of non-parametric trial-to-trial correlations between calcium responses and spiking responses for single-units in L4 and L2/3 in a naïve and an experience animal. Correlation values are z-scored by a shuffle control distribution (see methods for details). Units shown for the same age group belong to the same experiment and were therefore recoded simultaneously.

(C) Cumulative distribution of the strength and spatial spread of correlation with calcium responses for single-units recorded in L2/3 and L4 in naïve and experienced animals. ***: $p < 0.001$ for comparison across layers.

(D) Examples of direction tuning curves for single-units responses recorded in L2/3 and L4 of naïve and experienced animals. Solid lines represent trial-average responses. Dotted lines represent single-trial responses.

(E) Cumulative distribution of the orientation selectivity and discriminability of single-units responses recorded in L2/3 and L4 in naïve and experienced animals. ***: $p < 0.001$ for comparison across layers.

Figure 2

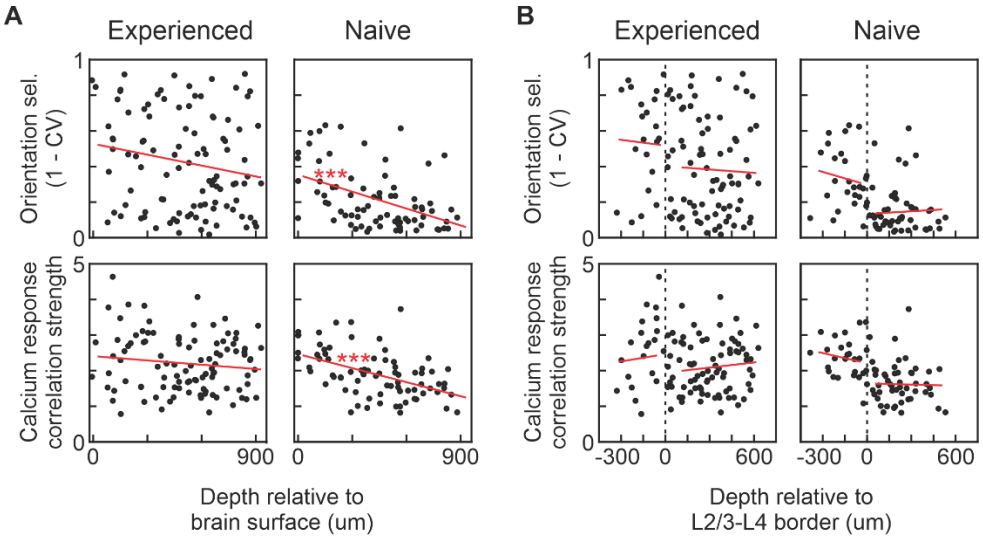

Figure 2: Single-unit response orientation selectivity and their correlation with calcium responses decrease with cortical depth and fall sharply at the layer 2/3 to layer 4 border in naïve but not experience V1.

(A) Scatter plots showing the relationship between the orientation selectivity or correlation with calcium responses of single-units and their cortical depth relative to brain surface forr all units recorded in naïve and experienced animals. Red lines show linear fits between unit's depth and the corresponding response property. ***: $p < 0.001$ for Pearson correlation between unit's depth and corresponding response property.

(B) Same as (A) but depth is calculated relative to the layer 2/3 (L2/3) to layer 4 (L4) border. Red lines show linear fits for single-units on either side of the laminar border.

Figure 3

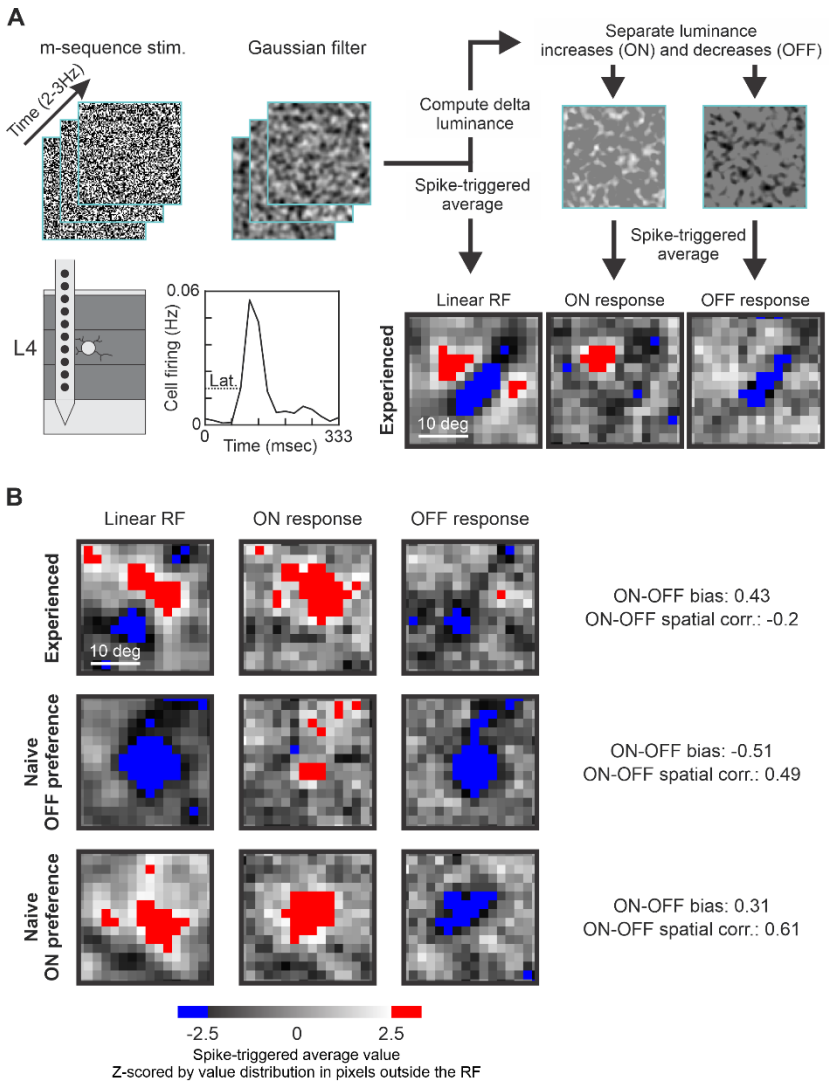

Figure 3: Using m-sequence stimuli to map linear receptive fields and analyze ON and OFF responses of layer 4 single-units across development.

(A) Diagram of experimental design and data analysis. Single-unit extracellular recordings were performed in layer 4 (L4) and responses to random m-sequence stimuli were recorded. Response latency was measured independently for each single-unit and corrected for in the following analysis. Stimuli were smoothed with a Gaussian filter (σ = 2deg) and a spike-triggered stimulus averaged computed to reveal the linear receptive field. In parallel, luminance difference was computed across adjacent frames of the m-sequence stimuli (after filtering) and ON and OFF responses were calculated as a spike-triggered averaged of increases and decreases in luminance respectively (see methods for details). Images show results for an example cell recorded on an experienced animal.

(B) Examples of linear receptive fields (RF) of one single-unit recorded in an experienced animal (top row) and two units, one displaying stronger OFF response (middle row) and one displaying stronger ON response (bottom row), recorded in naïve animals. Naïve examples illustrate how spatially superimposed ON and OFF responses result in a RF with a single sub-field of either polarity.

Figure 4

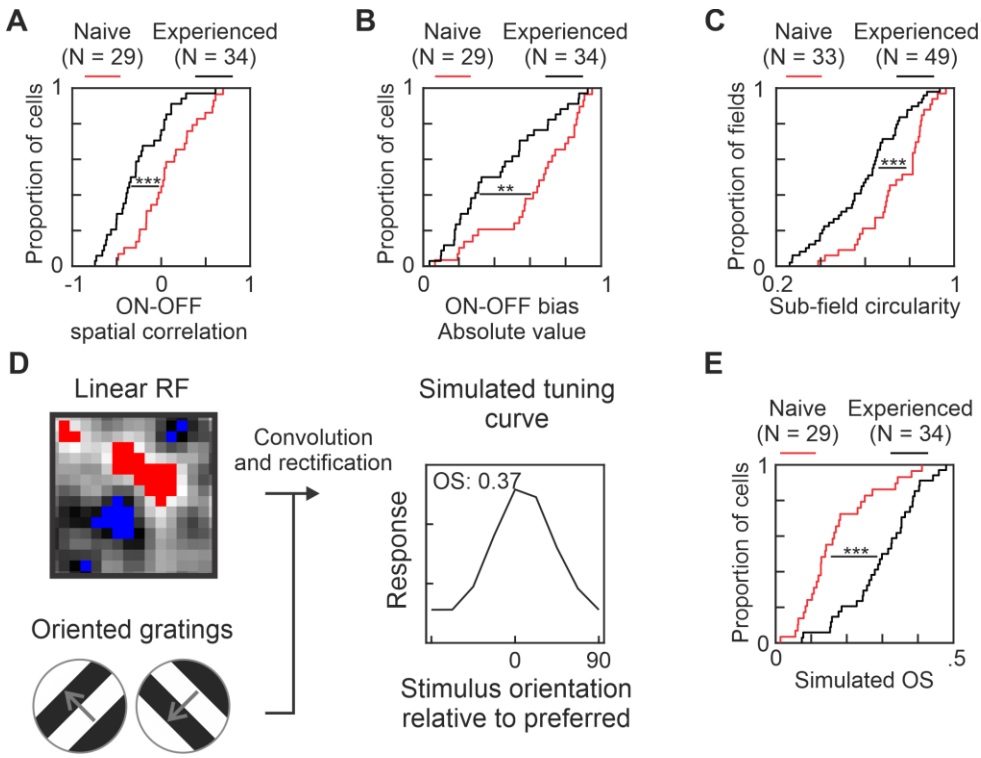

Figure 4: ON-OFF responses become spatially segregated in layer 4 after eye opening increasing the ability of the receptive field to detect edge orientation.

- *(A) Cumulative distribution of the correlation in spatial profile between ON and OFF responses for single-units recorded in layer 4 of naïve and experienced animals. Positive values indicate spatial superposition while negative values indicate spatial segregation. ***: p < 0.001 for comparison across age.*
- *(B) Cumulative distribution of the strength bias between the ON and OFF response for layer 4 single-units recorded in naïve and experienced animals. 1 indicates complete dominance of one polarity while 0 indicates equal strength between the responses. **: p < 0.01 for comparison across age.*
- *(C) Cumulative distribution of the circularity of ON and OFF sub-fields, computed as the ratio between their minor and major axis, in the linear receptive fields (RF) for layer 4 single-units recorded in naïve and experienced animals. ***: p < 0.001 for comparison across age.*
- *(D) Diagram of analysis to assess the ability of RF to detect edge orientation. Responses to oriented, drifting gratings were simulated by convolving the stimuli with the RF and applying a rectification to the resulting signal (see methods for details). Simulated orientation selectivity was then computed from the resulting response tuning curve.*
- *(E) Cumulative distribution of the simulated orientation selectivity (OS) of RF for layer 4 single-units recorded in naïve and experienced animals. ***: p < 0.001 for comparison across age.*

Figure 5

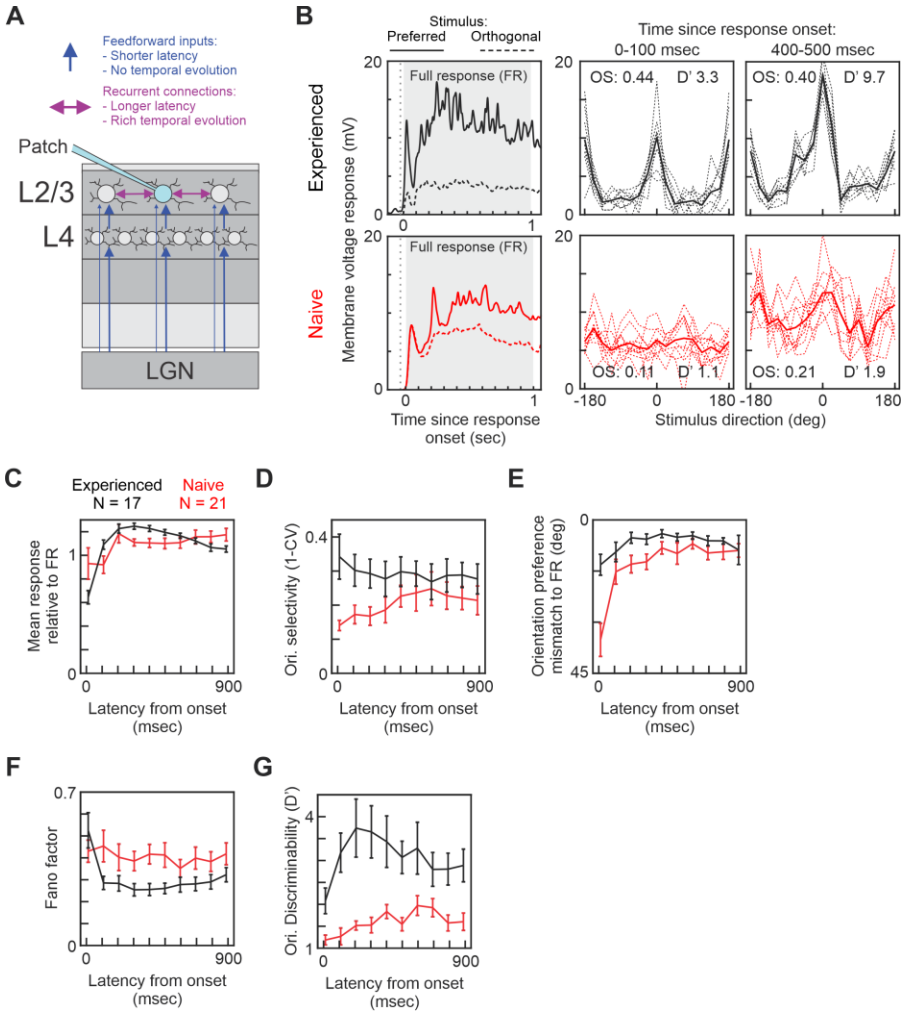

Figure 5: Feedforward inputs to layer 2/3 neurons become orientation selective and aligned with the layer 2/3 recurrent network after eye opening.

- *(A) Diagram of in-vivo whole-cell recording in layer 2/3 neurons. Blue arrows represent feedforward inputs, which are short-latency and dominate the earliest sub-threshold responses. Violet arrows represent recurrent connections, which act at longer-latencies and contribute to the temporal evolution of sub-threshold responses.*
- *(B) Data from example cells in an experienced and a naïve animal. Left graphs show sub-threshold responses over time to a drifting grating at the preferred orientation and direction (solid line) and to gratings of orthogonal orientation moving on either direction (dashed line). Shaded region represents full response averaged across 1 second following response onset. Doted gray line indicates the time of stimulus onset, which precedes response onset. Graphs to the right show trial averaged (solid line) and single trial (dotted lines) direction tuning curves for sub-threshold responses during a 100msec window starting at different latencies from response onset. OS: Orientation selectivity (1 – circular variance). D': Orientation discriminability.*
- *(C) Mean response (across stimuli and trials) at different latencies (100msec temporal window) relative to that of the full response. Line represents average across all cells recorded in naïve and experienced animals and error bars represent standard error.*
- *(D) Same as C for the orientation selectivity or responses at different latencies. CV: circular variance.*
- *(E) Same as C for the mismatch (absolute difference) between the orientation preference of responses at different latencies and that of the full response.*
- *(F) Same as C for the Fano factor (variance over mean) of the response to the preferred stimulus at different latencies.*
- *(G) Same as C for the orientation discriminability or responses at different latencies.*

Acknowledgements
We would like to thank C. Tepohl, J. Drayer, G. Kreal, R. Satterfield and N. Shultz for technical assistance, as well as members of the Fitzpatrick laboratory for helpful discussions. This research was supported by US National Institutes of Health grant EY011488 and EY026273, as well as the Max Planck Florida Institute for Neuroscience.

Author contributions
Both authors of this study worked on experimental design, results interpretation, and wrote the manuscript. A.A.L performed all experiments and data analysis.

Author information
The authors declare no competing financial interests. Correspondence and requests for materials should be addressed to D.F. (david.fitzpatrick@mpfi.org).

Code availability
The code for data analysis is available from the corresponding author upon request.

Data availability
The data that support the findings of this study are available from the corresponding author upon reasonable request.